NANO LETTERS

pubs.acs.org/NanoLett Letter

Ab Initio Design, Shaping, and Assembly of Free-Standing Silicon Nanoprobes

Zongguang Liu, Jiang Yan, Haiguang Ma, Tiancheng Hu, Junzhuan Wang, Yi Shi, Jun Xu, Kunji Chen, and Linwei Yu*

Cite This: *Nano Lett.* 2021, 21, 2773–2779 Read Online

ACCESS | Metrics & More | Article Recommendations | Supporting Information

ABSTRACT: Free-standing silicon nanoprobes (SiNPs) are critical tools for intracellular bioelectrical signal recording, while a scalable fabrication of these tiny SiNPs with *ab initio* geometry designs has not been possible. In this work, we demonstrate a novel growth shaping of slim Si nanowires (SiNWs) into SiNPs with sharp tips (curvature radii <300 nm), tunable angles of 30°, 60°, to 120° and even programmable triangle/circular shapes. A precise growth integration of orderly single, double, and quadruple SiNPs at prescribed locations enables convenient electrode connection, transferring and mounting these tiny tips onto movable arms to serve as long-protruding (over 4−20 μm) nanoprobes. Mechanical flexibility, resilience, and field-effect sensing functionality of the SiNPs were systematically testified in liquid nanodroplet and cell environments. This highly reliable and economic manufacturing of advanced SiNPs holds a strong potential to boost and open up the market implementations of a wide range of intracellular sensing, monitoring, and editing applications.

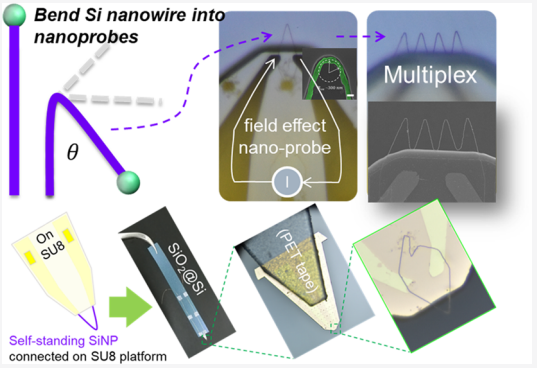

KEYWORDS: *Si nanoprobe, on-demand growth, ab initio design, scalable fabrication*

Quasi-one-dimensional (1D) silicon nanowires (SiNW) are ideal channel materials for the construction of highly sensitive field-effect biosensors[1−5] due to their large surface-to-volume ratio and the convenient electric readout scheme of the narrow 1D semiconducting channels. Recently, this benefit has been extended to probe the intracellular electric signals in living cells,[6] where the SiNWs need to be folded into free-standing nanoprobes (NPs), as diagrammed schematically in Figure 1a,[7] forming pointy tips to touch and penetrate targeted cells. Compared to the patch-clamp pipet electrodes, the inserted SiNP tip establishes a highly localized circuit loop or endocytic pathway that records the intracellular signals only at the specific cell regions or subcellular structures without the need for solution exchange.[8−11] More importantly, the nanoscale SiNP/membrane contact leads to minimal invasiveness, thus holding the potential to establish a biofriendly high spatiotemporal resolution tool for the physiological investigation of neural and cardiac cells.[12−15]

However, folding SiNWs into SiNPs of desired geometry is not an easy task. The first SiNPs were fabricated by taking advantage of the kinked growth of SiNWs during vapor−liquid−solid (VLS) process,[16,17] with basically fixed turning angle of 60° determined by the crystallographic orientation in c-Si lattice. As the kinked SiNWs (SiNPs) are usually grown as random vertical bundles, they have to be broken, selectively transferred, and connected via costly and low-yield procedures, such as pick-and-place manipulation and the use of elaborated electron beam lithography (EBL).[13] The straight SiNWs can also be dispersed in solution and flushed over prepatterned substrate surface to be captured by convex trenches and forced to bend into U-shape tips.[18] Despite of the successful demonstrations of SiNP biointerfacing and sensing functionalities (Figure 1b),[18] achieving a more precise and complex tip geometry control, with even sharper tips (curvature radius <500 nm), are certainly beneficial and desirable. Actually, the tip shapes and curvatures of the SiNPs are found to have significant impact on the integrity and merging dynamics at the probe/membrane interface[19,20] and could provide a novel basis to develop new cell manipulation functionalities. In view of fulfilling the potential of SiNPs, an *ab initio* geometry control of the SiNPs in terms of the turning angle, tip shape, and multiplex arrangement, as depicted in Figure 1c, is highly desirable but has not been accomplished so far. Meanwhile, a scalable, high-yield, and designable manufacturing of the tiny

Received: December 5, 2020
Revised: March 10, 2021
Published: March 17, 2021

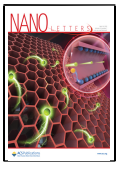

https://doi.org/10.1021/acs.nanolett.0c04804
Nano Lett. 2021, 21, 2773−2779

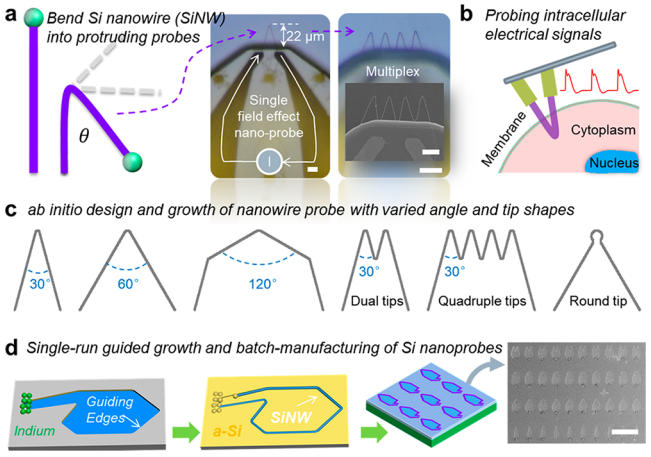

Figure 1. Free-standing Si nanoprobes (SiNPs) for intracellular electrical signal detection. (a) Transformation of straight Si nanowires (SiNWs) into bending SiNPs, as accomplished here by planar growth of SiNWs and shown in the photo and scanning electron microscopy (SEM) images shown in the right panels. (b) The use of SiNP to record the electric signal variation in cells. (c) *Ab initio* design of the SiNPs with different angles and tip shapes. (d) Batch fabrication procedure of orderly SiNP array via planar guided growth of SiNWs along predesigned guiding edges, which include first a H_2 plasma treatment of the indium (In) pads, transforming them into discrete droplets, followed by the coating of amorphous Si (a-Si) layer as precursor. After annealing growth at higher temperature, the remnant a-Si layer was selectively etched off, leaving the structure as seen in the SEM image shown in the rightmost panel. Scale bars in (a) and inset are 10 μm and in (d) is 100 μm.

SiNPs is also the key to promote this new nanoprobe technology and its widespread practical applications.

In this work, we demonstrate a highly programmable growth shaping and assembly of functional SiNP tips, based on an in-plane solid−liquid−solid (IPSLS) mechanism established in our previous works,[21−25] which enables a scalable manufacturing of orderly SiNP array without the use of any high-precision EBL technology. Thanks to the preknown locations and orientations, the as-grown SiNPs with preferred sharp turning angles can be easily assembled and connected upon maneuverable arms to serve as free-standing probes for local field effect probing/sensing. A scalable fabrication and assembling of the suspended and sophisticated SiNPs, as well as their mechanical and electric properties as functional probes, have never been demonstrated or investigated in our previous works.

RESULTS AND DISCUSSION

Growth Shaping of Si Nanoprobes. The fabrication procedure is illustrated schematically in Figure 1d which involves, first, the patterning of step edges by etching 150 nm deep into the underlying wafer substrate precoated with 600 nm SiO_2 layer (Supporting Information (SI) Section 1.1), followed by the evaporation of In catalyst pads at the ends of the guiding steps via conventional lithography, thermal evaporation, and lift-off procedure. Then, after loading into a plasma-enhanced chemical vapor deposition (PECVD) system, a H_2 plasma treatment was applied to transform the In pads into discrete droplets at ∼250 °C. After that, the whole surface was coated with an amorphous Si (a-Si) layer, deposited by pure SiH_4 plasma at a lower substrate temperature 150 °C (below the melting point of In). In the next step, the substrate was heated to 350 °C to activate the molten In droplets to absorb the a-Si layer to produce crystalline SiNWs. During this IPSLS growth, the extra a-Si coated on the vertical sidewalls of

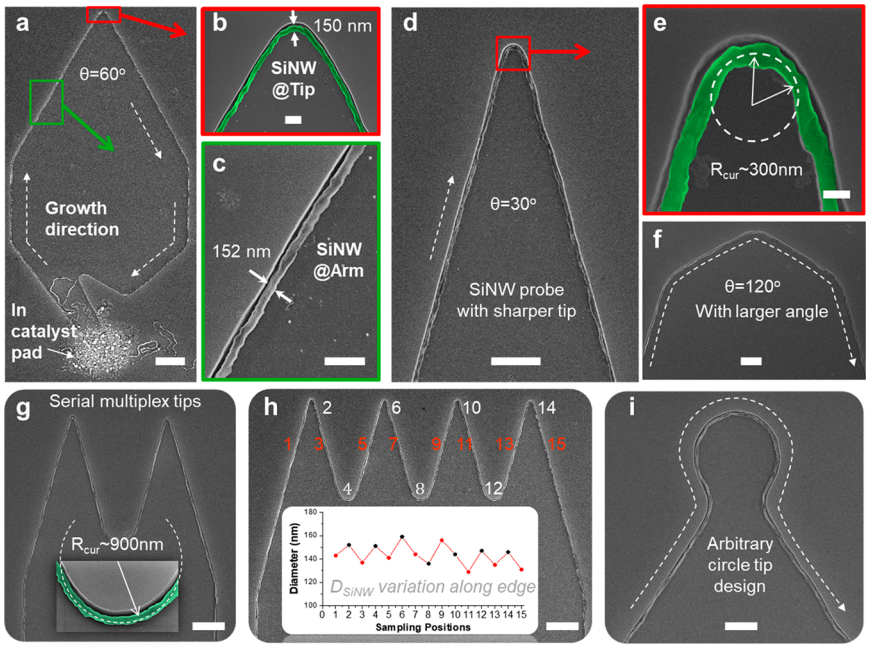

Figure 2. Growth shaping of SiNW nanoprobes via step-edge guiding strategy. (a) Guided growth of a SiNW probe with tip angle of 60° with enlarged SEM views of the bending tip and the straight arm shown in (b) and (c). Scale bars in (a−c) are 10 μm, 500 nm, and 500 nm, respectively. (d) Sharper SiNW probe with tip angle of 30° and curvature radius of R_{cur} ∼ 300 nm (see panel e); (f) wider probe with a tip angle of 120°. Scale bars in (d−f) are 2 μm, 200 nm, and 2 μm, respectively. (g−i) Single-run growth shaping of multiplex (double in (g) and quadruple in (h)) and round in (i) probe tips. Scale bars in panels g−i are 2 μm. The inset in (h) displays the diameter variation sampled at the straight (red) or bending (black) locations.

https://doi.org/10.1021/acs.nanolett.0c04804
Nano Lett. 2021, 21, 2773−2779

the step edges can help to attract and direct the movement of the leading In droplets, and thus producing SiNWs along the guiding edges.[22,26,27] Compared to the relatively short, straight, and simple SiNW array grown in our previous works to serve as 1D channels for FET devices,[27,28] the long SiNWs here are purposely grown and tailored into specific probe shapes with various preferable angles and sharp tips, as seen, for example, in Figure 1, which is indispensable to enable and promote the biofriendly high spatiotemporal resolution tool for physiological investigation of neural and cardiac cells. Finally, the remnant a-Si layer can be removed selectively by H_2 etching, leaving only the crystalline SiNWs. More experimental details and explanations of the guided growth mechanism are provided in the Experimental Section or our previous works.[28−31]

The typical SEM images of the as-grown SiNPs are presented in Figure 2, where controlling the planar growth of the SiNWs into tunable tip shapes and angles has been accomplished by using different prepatterned guiding edge designs. For example, the SiNPs with tip angles of $\theta = 30°$, 60°, and 120° are showcased in Figure 2a,d,f, respectively, which is not constrained by the fixed twin angles (60° or 120°) for the VLS grown SiNPs,[12,16,17,32] enabling thus a critical new dimension of control the SiNPs that has not been possible before. More importantly, complex multiplex and round tips can be manufactured via a single run growth of ultralong SiNWs, as seen in the SEM images shown in Figure 2g−i. Note that these advanced tip geometries that cannot be fabricated via the kinked VLS growth[13,33] or brush-bending approaches[18,19] might find advantageous applications in developing more sophisticated and advanced bioprobing, manipulation, or synchronic multichannel sampling functionalities.

Close SEM scrutiny of the SiNPs reveals that the slim SiNWs with typical diameter of $D_{nw} \sim 150$ nm and length $L_{nw} > 200$ μm are grown out of the crossing edges of the In pad and the guiding steps (Figure 2a). Only the SiNWs that get trapped and directed by the guiding edges can travel a long distance over the full contour of the nanoprobes, while the other random SiNWs stretching out of the In pads are mostly self-trapped and stopped at the nearby regions. As a prerequisite to produce self-standing SiNPs, the planar growth of SiNWs has to be continuous and stable, following the guiding edge lines, which have been checked and confirmed at several typical locations, such as at the straight arms and the bending tips locations, as seen in Figure 2b,c, respectively. According to the diameter samplings along a SiNW grown over a four-tip-probe profile, as seen in Figure 2h, this specific SiNW has a mean diameter of ∼140 ± 9 nm and becomes slightly thicker at the convex or concave turning locations. Much thinner SiNWs with diameter down to <50 nm can also be grown along the guiding edge, as seen, for example, in Figure S1a,b, with the use of smaller In catalyst droplet and proper parameter control over the a-Si layer thickness and step height. Even without the use of elaborated EBL etching technology, the radii of curvature (ROC) at the tips can be scaled down to only $R_{cur} \sim 300$ nm at the concave tip (see Figure 2e) with a predesigned bending angle of 30°, which is much smaller than the typical size of the patch-clamp micropipette (∼1 μm in diameter).[34,35] In addition, the ROC can be further reduced to only 200 nm (see Figure S1c) when the intersect angle of the guiding edges is decreased to 20°. It has been know that a sharper SiNP tip offers a beneficial quasi 1D contact to the cell membrane, causing a larger degree of local stretching/bending to trigger membrane fusion, as it works to relax the tension,[20] and providing a mild probe-cell interface with the least invasiveness during cellular recording. On the other hand, it is important to emphasize that this delicate and programmable fabrication has been accomplished by using only conventional high-throughput lithography with spatial resolution of ∼2 μm and inductive coupled plasma (ICP) etching. Under the current experimental conditions, the successful growth rate for having ultralong SiNWs lying along the contours of the nanoprobe is ∼90%, providing a solid basis for achieving a scalable batch-manufacturing of designable SiNPs with a novel high geometry control precision and at extremely low cost.

Assembling Suspended SiNPs. The SiNP array grown on the SiO_2-coated wafer substrates were first connected by Pt/Au metal electrode pads, made via photolithography, evaporation, and lift-off procedure, as depicted in Figure 3a.

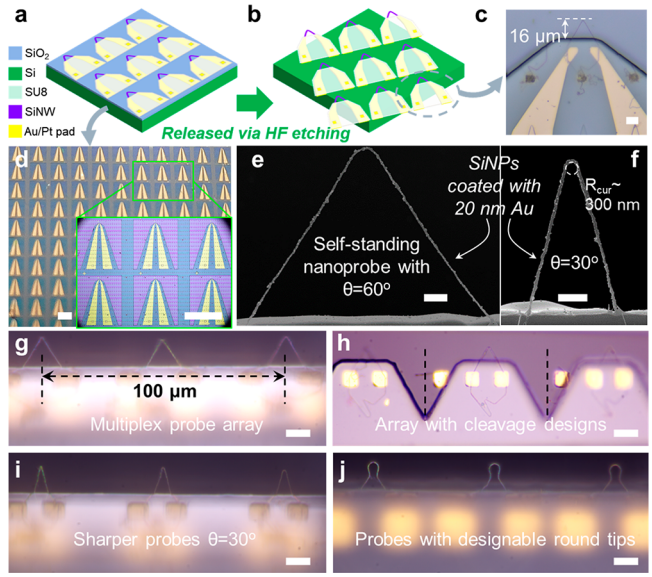

Figure 3. Scalable assembly of free-standing SiNPs. (a,b) Electric connection, SU8 coating, and transferring of the orderly SiNP array with an optical image of the array presented in (c) and a close examination in (d), revealing a suspended SiNP that extends ∼16 μm away from the SU8 holding edge. (e,f) SEM images of the free-standing SiNPs with tip angles of 60° and 30°, respectively. (g−j) Photo images of the transferred SiNP array with different tip angle and shape designs. Scale bar in (c) is 10 μm, in (d) and inset are 1 mm, in (e,f) are 2 μm, and in (g−j) are 10 μm.

Then, a supportive SU8 framework of 20 μm thick was spin-coated and patterned, covering the metal pads and holding the SiNPs at the roots. A photograph of a 110 (10 × 11) array of SiNPs, covered with SU8/metal pads, is shown in Figure 3d with an enlarged view displayed in the bottom-right inset, showing more details of the interconnected framework of the SiNP units. After that, the SiNPs were released from the parent substrate, by etching off the underlying SiO_2 layer, and transferred to movable robot arms, as illustrated schematically in Figure 3b. A typical photo image of the transferred and suspended SiNP is presented in Figure 3c, which extends ∼16 μm away from the SU8 holding edge. Note that the only electric connection path between the two electrode pads is through the upper SiNP tip, as the SiNWs grown along the lower guiding edges are not connected because of the self-

https://doi.org/10.1021/acs.nanolett.0c04804
Nano Lett. 2021, 21, 2773−2779

avoiding growth nature of the planar SiNWs.[21,36] Moreover, the multiplex probe array can also be grown in single run and connected by five separate electrodes, as seen Figure S2, which are the ideal multichannel detectors to monitor/trace the distribution and propagation of intracellular signals, as demonstrated already by Zhao and et al. in their previous work.[19]

The free-standing SiNPs can also be observed by using SEM, as seen in Figure 3e,f, but where a thin layer of Au (nominally 20 nm, appearing as granules on the SiNWs) has to be sputtered to disperse the surface charge accumulated on the insulating SU8 holder surface. The SEM images confirm again the very well-defined slim SiNP profile with a rather sharp tip down to $R_{cur} \sim 300$ nm, without the use of costly and inefficient EBL lithography. Furthermore, thanks to the precise location controls, SiNPs of different tip geometries can be easily fabricated and assembled asa multiplex probe array, as witnessed in Figure 3g–j, indicating a reliable and high yield procedure that can accomplish a precise growth/assembling control over huge dimension scales, spanning from nanometers to millimeters.

Mechanical Stability and Resilience of SiNPs. As the SiNPs are supposed to work as resilient tools to pierce the cell membrane and probe the intracellular signals, the mechanical properties of the suspended nanoprobes are of great concern but seldom addressed in prior investigations. To test the resilience and deformation, a free-standing SiNP with suspended extension of $L_{NP} = 16$ μm, as seen in Figure 4a,

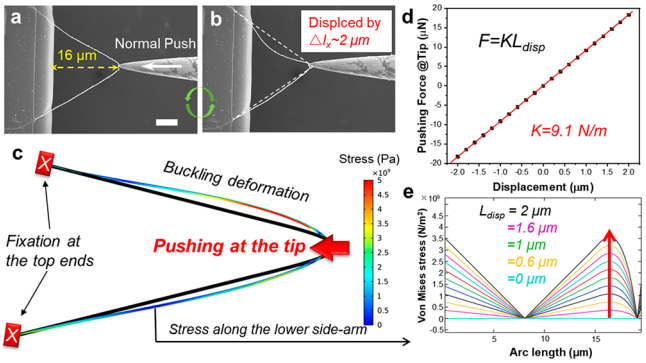

Figure 4. Mechanical property and resilience testing of suspended SiNP. (a,b) SEM images of a SiNP prior and after normal pushing to a displacement of $\Delta l_x = 2$ μm, respectively. Scale bar is 5 μm. (c) Finite element simulation and stress profile of the SiNP under pushing displacement to 2 μm, viewed at 45° tilted angle, while (d,e) plot the calculated force–displacement response of the SiNP and the stress distributions extracted along the lower side arm under different pushing displacement.

was loaded into SEM chamber and pushed by a tungsten tip in normal or x-direction. Under pushing to $\Delta l_x \sim 2$ μm, corresponding to 12.5% strain (Figure 4b), both the SiNW arms demonstrate obvious buckling deformation to accommodate the imposed pushing force at the tip. When the pushing retreated, the SiNP can still recover to its original form. Meanwhile, the SiNP can also accommodate large side-pushing to $\Delta l_y > 3.5$ μm, as shown in Figure S3. Note that the thin Au coating on the SiNP sidewall, as tiny granular decorations to improve SEM imaging, is not supposed to modify significantly the mechanical property of the probe structure (more discussion provided in SI Section 1.2). These observations highlight the excellent resilience and mechanical stability of the SiNPs under significant pushing and deformation. The structural deformation was further analyzed by using finite element simulation toolkit COMSOL, which can help to estimate the stress distribution along the SiNW arms under normal pushing or pulling strain, as shown in Figure 4c and Figure S4, respectively. Under the enforced pushing or pulling displacement, the SiNP behaves like a linear spring, as plotted in Figure 4d, featuring a resilient coefficient of $F = kL_{disp}$ with $k = 9.1$ N/m. The maximal stress appears, extracted along the lower arm and presented in Figure 4e, at the buckled region and the fixed ends, approaching to 3.5 GPa under the maximal pushing displacement to $\Delta l_x = 2$ μm, which is still within the fracture limit of 2–10 GPa for c-Si.[37] However, in reality both the two fixations of SiNP to the SU8 holder edge and the top contact to the membrane are relatively soft, thus high fracture risk is mostly limited to the buckled segment on the two arms. Nevertheless, as the typical force required to pierce the plasma membrane (with a thickness of 6 nm) with a contact size of $\sim 10^2$ nm^2 is only in the range of $\sim 10^{-9}$ N or nN,[38] the SiNP that can exert safely normal stress force > μN (Figure 4d) should be considered as stiff/sharp enough to penetrate easily the lipid membrane (more discussion is presented in SI Section 1.3).

Probe Connection, Manipulation, and Sensing Testing. In order to testify the sensing functionality in liquid and cell environment, a free-standing SiNP/metal/SU8 unit was mounted onto a piece of c-Si strip holder 0.6 cm × 6 cm as shown in Figure 5a,b, which was cut out of Si wafer precoated with 600 nm SiO_2 on both sides and connected to the probe via an insulated polyethylene terephthalate (PET) tape. Enlarged views of the assembled probe and the suspended SiNW tip structures are provided in Figure 5c,d, respectively. Electric connection to the metal pads on the SU8 holder was realized by using silver paste and soft Au thread, and after fixing the whole structure on a movable stage (see Figure 5f), the electric signals were connected to and measured by a high precision Keithley 2636B source-monitor unit (SMU, U.S.A.). Figure S5 presents the current versus voltage (IV) characteristics for 12 different SiNP devices in dry environment, showing a mean resistance of 31.6 ± 6.7 MΩ. After coating the SiNP with 30 nm Al_2O_3 layer, the field effect sensing was first tested by approaching and penetrating the SiNP into separated tiny droplets with different pH values. As shown in Figure 5e, the SiNP channel current jumps quickly, by more than 300%, upon touching the liquid droplet surface and then experiences a slow decay prior to arriving at a stable response stage. After retreating the SiNP from liquid droplet, the channel current resumes quickly back to its original state. In general, higher pH values lead to higher channel current, indicating a field effect gating or sensing of the SiNP channel. This is also consistent with the expectation that the IPSLS SiNWs are slightly p-type due to the incorporation of In catalyst atoms.[22,39] High concentration of OH^- is supposed to boost the conductivity of the p-type SiNW channel, as observed indeed in the SiNW FET devices. In addition, the SiNP was also manipulated to penetrate living mesenchymal stem cells, see Figure 5g, with an aim to test the mechanical stability of the SiNP during their interaction with more complicated nanoscale objects. As we can see, the sharp SiNP can be precisely maneuvered over the cell, approach the targeted cell, and touch down to pierce into the cells, although the distortions of the cell membrane are rather difficult to resolve as they look basically transparent

https://doi.org/10.1021/acs.nanolett.0c04804
Nano Lett. 2021, 21, 2773–2779

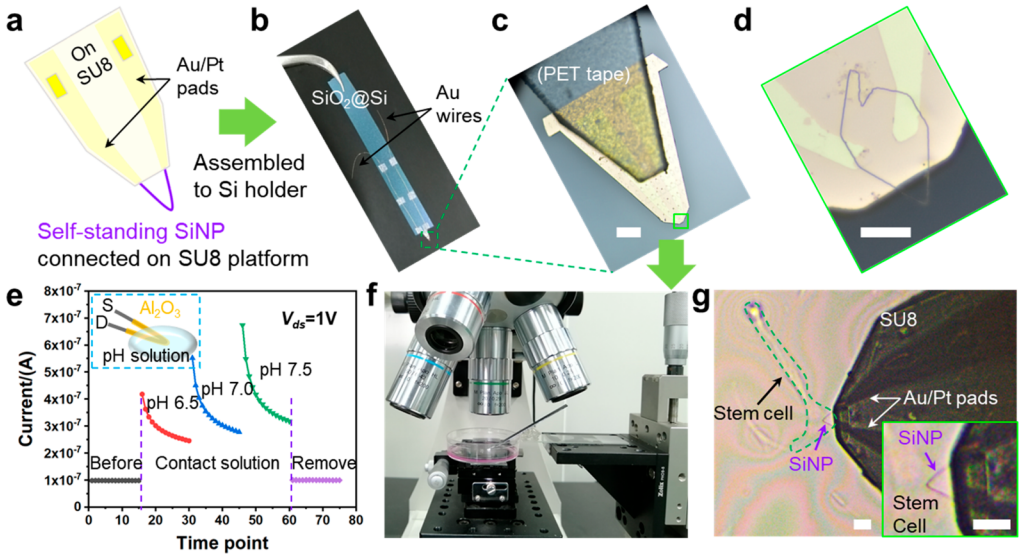

Figure 5. Fabrication, manipulation, and mechanical characterization of the free-standing probe. (a–c) The assembling of the free-standing probe by striplike silicon substrate connected by an insulated PET tape. (d) The optical image of the fabricated free-standing probe. (e) The sensor properties of the fabricated SiNW-FET probe in pH solution. (f,g) The free-standing probe was mounted on an XYZ micromanipulator and targeted to the elected stem cell. Scale bar in (c) is 200 μm, in (d), (g), and inset are 20 μm.

under the optical microscopy. More discussions about the cell viability after SiNP puncturing and the potential use of multiplex SiNPs are provided in SI Sections 1.4 and 1.5, respectively. Although action potential and intracellular signal recordings could not be accomplished in our lab at this moment, mainly due to the lack of key specialized experimental setups and reliable/convenient cell culturing environments, the key capabilities demonstrated here, such as *ab initio* designing, precise batch-manufacturing, and assembling of the tailored SiNWs to serve as self-suspended nanoprobes and approach/touch the miniature targets, provide a solid basis for future more systematic and comprehensive intracellular and neural system investigations, as demonstrated already with the use of kinked and bent Si nanoprobes.[12,13,19]

CONCLUSION

In summary, a scalable and programmable growth-shaping manufacturing and assembly of self-standing SiNPs have been demonstrated which enables a novel *ab initio* control of tip geometry with curvature radii ~300 nm, tunable angles of 30°, 60° to 120° and designable triangle or circular shapes. Orderly single, double, and quadruple multiplex SiNPs can be reliably grown at prescribed locations, connected and transferred onto movable arms with large free-standing extension of 4–20 μm. Mechanical resilience and field-effect sensing functionality of the SiNPs were examined in straightforward pushing test and verified in liquid droplet and cell environments, respectively. These results have the potential to enable a wide range of new intracellular sensing, monitoring, and editing applications.

EXPERIMENTAL SECTION

Growth of SiNW by IPSLS. The SiNWs were grown upon SiO_2-coated Si wafers substrates via an IPSLS growth mechanism. Briefly, guiding step edges with predesigned probe geometry were first defined by photolithography and etched into the SiO_2 layer by using inductively coupled plasma to a depth of 90–150 nm. In stripes of 30 nm thick were deposited by thermal evaporation and lift-off procedure at the starting ends of guiding edges. Next, a hydrogenated amorphous Si (a-Si) thin film is deposited upon a substrate surface to serve as the precursor layer, which is absorbed by In catalyst droplets to produce crystalline SiNWs. Then samples were loaded into a PECVD system and treated with a H_2 plasma at 250 °C for 5 min with gas flow rate and chamber pressure of 15 sccm and 140 Pa, respectively. The substrate temperature was decreased to 150 °C, and the a-Si thin film was deposited below the melting point of the In catalyst with 5 sccm pure SiH_4 plasma with 20 Pa pressure for 7 min. The substrate temperature was raised to 350 °C and kept in vacuum for 60 min; the In droplets started to grow by converting the a-Si layer into crystalline SiNWs. At the end of the SiNW growth, the remnant a-Si layer was selectively etched off by using H_2 plasma at around 120 °C.

Nanoprobe Fabrication and Measurement. Platinum/gold (5/55 nm) contacts were fabricated by ultraviolet lithography and followed by magnetron sputtering and lift-off process. Before sputtering, the SiNWs were treated by hydrofluoric acid (4%) for 20 s to remove the oxide layer. The electrodes were covered with an upper SU-8 layer by lithography and baked under 135 °C for 2 h. Subsequently, the samples were treated in hydrofluoric acid solution (4%) to release the probe by etching under the SiO_2 layer, followed by critical point drying. The probes supported by SU-8 were transferred onto a target substrate and then passivated by Al_2O_3 layer (30 nm) by atomic layer deposition to construct the SiNW FET. The silver paste was used to connect the Au electrode and detected circuit. Scanning electron microscope (SEM, Zeiss Sigma) and optical microscope were used to characterize key steps in the SiNW growth and probe fabrication flow. For electrical characterization, one arm of the SiNW-FET was considered as the source, and the other arm was considered as the drain. Electrical transport studies in phosphate buffered saline with various pH value (6.5, 7.0, and 7.5) were carried out using a Source-Meter to characterize the sensor properties at a constant voltage (1 V).

Mechanical Testing and Finite Element Simulation. A metal tungsten probe with the tip radius of ~150 nm was

https://doi.org/10.1021/acs.nanolett.0c04804
Nano Lett. 2021, 21, 2773–2779

mounted on the manipulator installed within the SEM chamber, which then was used to contact and push the SiNP tip in normal direction or from its sidewall. The deformations of the SiNP under different tungsten-tip-imposed strains were captured in real time by SEM observation. The finite element simulation of the free-standing SiNP, as shown in Figure 4c and Figure S4, were carried out by using COMSOL simulation toolkits. The geometry dimensions (such as diameter, arm length, curvature) were extracted from the SEM observation shown in Figure 4a, while the material of the SiNW was assumed to be anisotropic c-Si with Young's modulus of 160 GP, Poisson's ratio of 0.22, and density of 2329 kg/m^3.

■ ASSOCIATED CONTENT

Supporting Information

The Supporting Information is available free of charge at https://pubs.acs.org/doi/10.1021/acs.nanolett.0c04804.

Growth of SiNW; mechanical property of SiNP; exact force for cell puncturing; cell viability after SiNP puncturing; potential use of multiplex SiNPs; (Figure S1) guided growth of ultrathin SiNWs; (Figure S2) optical image of the multiplex probe; (Figure S3) mechanical property testing of suspended SiNP under side-pushing; (Figure S4) calculated stress distribution of the SiNP under pulling strain at the tip by finite element simulation; (Figure S5) electrical performances of the SiNP (PDF)

■ AUTHOR INFORMATION

Corresponding Author

Linwei Yu − *National Laboratory of Solid State Microstructures, School of Electronics Science and Engineering, Collaborative Innovation Center of Advanced Microstructures, Nanjing University, Nanjing 210093, P.R. China;* orcid.org/0000-0002-0801-5210; Email: yulinwei@nju.edu.cn

Authors

Zongguang Liu − *National Laboratory of Solid State Microstructures, School of Electronics Science and Engineering, Collaborative Innovation Center of Advanced Microstructures, Nanjing University, Nanjing 210093, P.R. China;* orcid.org/0000-0003-4141-7462

Jiang Yan − *National Laboratory of Solid State Microstructures, School of Electronics Science and Engineering, Collaborative Innovation Center of Advanced Microstructures, Nanjing University, Nanjing 210093, P.R. China*

Haiguang Ma − *National Laboratory of Solid State Microstructures, School of Electronics Science and Engineering, Collaborative Innovation Center of Advanced Microstructures, Nanjing University, Nanjing 210093, P.R. China*

Tiancheng Hu − *National Laboratory of Solid State Microstructures, School of Electronics Science and Engineering, Collaborative Innovation Center of Advanced Microstructures, Nanjing University, Nanjing 210093, P.R. China*

Junzhuan Wang − *National Laboratory of Solid State Microstructures, School of Electronics Science and Engineering, Collaborative Innovation Center of Advanced Microstructures, Nanjing University, Nanjing 210093, P.R. China*

Yi Shi − *National Laboratory of Solid State Microstructures, School of Electronics Science and Engineering, Collaborative Innovation Center of Advanced Microstructures, Nanjing University, Nanjing 210093, P.R. China*

Jun Xu − *National Laboratory of Solid State Microstructures, School of Electronics Science and Engineering, Collaborative Innovation Center of Advanced Microstructures, Nanjing University, Nanjing 210093, P.R. China;* orcid.org/0000-0002-0469-9766

Kunji Chen − *National Laboratory of Solid State Microstructures, School of Electronics Science and Engineering, Collaborative Innovation Center of Advanced Microstructures, Nanjing University, Nanjing 210093, P.R. China*

Complete contact information is available at: https://pubs.acs.org/10.1021/acs.nanolett.0c04804

Notes

The authors declare no competing financial interest.

■ ACKNOWLEDGMENTS

The authors acknowledge the financial supports received from the National Natural Science Foundation of China under Nos. 11874198, 61674075, 61974064, and 61921005 and National Key R&D Program of China under Nos. 2018YFB2200101 and 2018YFA0209104, as well as the support from the Micro-Fabrication and Integration Technology Center in Nanjing University. Z.L. thanks the financial support from China Postdoctoral Science Foundation (2020M671440).

■ REFERENCES

(1) Zafar, S.; D'Emic, C.; Jagtiani, A.; Kratschmer, E.; Miao, X.; Zhu, Y.; Mo, R.; Sosa, N.; Hamann, H.; Shahidi, G.; Riel, H. Silicon nanowire field effect transistor sensors with minimal sensor-to-sensor variations and enhanced sensing characteristics. *ACS Nano* **2018**, *12*, 6577−6587.

(2) Shehada, N.; Cancilla, J. C.; Torrecilla, J. S.; Pariente, E. S.; Bronstrup, G.; Christiansen, S.; Johnson, D. W.; Leja, M.; Davies, M. P.; Liran, O.; Peled, N.; Haick, H. Silicon nanowire sensors enable diagnosis of patients via exhaled breath. *ACS Nano* **2016**, *10*, 7047−7057.

(3) Wang, B.; Cancilla, J. C.; Torrecilla, J. S.; Haick, H. Artificial sensing intelligence with silicon nanowires for ultraselective detection in the gas phase. *Nano Lett.* **2014**, *14*, 933−938.

(4) Cui, Y.; Wei, Q. Q.; Park, H. K.; Lieber, C. M. Nanowire nanosensors for highly sensitive and selective detection of biological and chemical species. *Science* **2001**, *293*, 1289−1292.

(5) Gao, A.; Lu, N.; Dai, P.; Li, T.; Pei, H.; Gao, X.; Gong, Y.; Wang, Y.; Fan, C. Silicon-nanowire-based CMOS-compatible field-effect transistor nanosensors for ultrasensitive electrical detection of nucleic acids. *Nano Lett.* **2011**, *11*, 3974−3978.

(6) Jiang, Y.; Tian, B. Inorganic semiconductor biointerfaces. *Nat. Rev. Mater.* **2018**, *3*, 473−490.

(7) Tian, B.; Lieber, C. M. Nanowired bioelectric interfaces: Foucus review. *Chem. Rev.* **2019**, *119*, 9136−9152.

(8) Chen, K. I.; Li, B. R.; Chen, Y. T. Silicon nanowire field-effect transistor-based biosensors for biomedical diagnosis and cellular recording investigation. *Nano Today* **2011**, *6*, 131−154.

(9) Liu, H.; Haider, B.; Fried, H. R.; Ju, J.; Bolonduro, O.; Raghuram, V.; Timko, B. P. Nanobiotechnology: 1D nanomaterial building blocks for cellular interfaces and hybrid tissues. *Nano Res.* **2018**, *11*, 5372−5399.

(10) Cohen-Karni, T.; Casanova, D.; Cahoon, J. F.; Qing, Q.; Bell, D. C.; Lieber, C. M. Synthetically encoded ultrashort-channel nanowire transistors for fast, pointlike cellular signal detection. *Nano Lett.* **2012**, *12*, 2639−2644.
(11) Parameswaran, R.; Tian, B. Rational Design of Semiconductor Nanostructures for Functional Subcellular Interfaces. *Acc. Chem. Res.* **2018**, *51*, 1014−1022.
(12) Xu, L.; Jiang, Z.; Mai, L.; Qing, Q. Multiplexed free-standing nanowire transistor bioprobe for intracellular recording: a general fabrication strategy. *Nano Lett.* **2014**, *14*, 3602−3607.
(13) Qing, Q.; Jiang, Z.; Xu, L.; Gao, R.; Mai, L.; Lieber, C. M. Free-standing kinked nanowire transistor probes for targeted intracellular recording in three dimensions. *Nat. Nanotechnol.* **2014**, *9*, 142−147.
(14) Duan, X.; Lieber, C. M. Nanoelectronics meets biology: from new nanoscale devices for live-cell recording to 3D innervated tissues. *Chem. - Asian J.* **2013**, *8*, 2304−2314.
(15) Duan, X.; Gao, R.; Xie, P.; Cohen-Karni, T.; Qing, Q.; Choe, H. S.; Tian, B.; Jiang, X.; Lieber, C. M. Intracellular recordings of action potentials by an extracellular nanoscale field-effect transistor. *Nat. Nanotechnol.* **2012**, *7*, 174−179.
(16) Tian, B.; Xie, P.; Kempa, T. J.; Bell, D. C.; Lieber, C. M. Single-crystalline kinked semiconductor nanowire superstructures. *Nat. Nanotechnol.* **2009**, *4*, 824−829.
(17) Jiang, Z.; Qing, Q.; Xie, P.; Gao, R.; Lieber, C. M. Kinked p−n junction nanowire probes for high spatial resolution sensing and intracellular recording. *Nano Lett.* **2012**, *12*, 1711−1716.
(18) Zhao, Y.; Yao, J.; Xu, L.; Mankin, M. N.; Zhu, Y.; Wu, H.; Mai, L.; Zhang, Q.; Lieber, C. M. Shape-controlled deterministic assembly of nanowires. *Nano Lett.* **2016**, *16*, 2644−2650.
(19) Zhao, Y.; You, S. S.; Zhang, A.; Lee, J. H.; Huang, J.; Lieber, C. M. Scalable ultrasmall three-dimensional nanowire transistor probes for intracellular recording. *Nat. Nanotechnol.* **2019**, *14*, 783−790.
(20) Fang, Y.; Tian, B. Curving neural nanobioelectronics. *Nat. Nanotechnol.* **2019**, *14*, 733−735.
(21) Yu, L.; Alet, P.-J.; Picardi, G.; Roca i Cabarrocas, P. An in-plane solid-liquid-solid growth mode for self-avoiding lateral silicon nanowires. *Phys. Rev. Lett.* **2009**, *102*, 125501.
(22) Yu, L.; Chen, W.; O'Donnell, B.; Patriarche, G.; Bouchoule, S.; Pareige, P.; Rogel, R.; Claire Salaun, A.; Pichon, L.; Roca i Cabarrocas, P. Growth-in-place deployment of in-plane silicon nanowires. *Appl. Phys. Lett.* **2011**, *99*, 203104.
(23) Xu, M.; Xue, Z.; Wang, J.; Zhao, Y.; Duan, Y.; Zhu, G.; Yu, L.; Xu, J.; Wang, J.; Shi, Y.; Chen, K.; Roca i Cabarrocas, P. Heteroepitaxial writing of silicon-on-sapphire nanowires. *Nano Lett.* **2016**, *16*, 7317−7324.
(24) Xue, Z.; Xu, M.; Zhao, Y.; Wang, J.; Jiang, X.; Yu, L.; Wang, J.; Xu, J.; Shi, Y.; Chen, K.; Roca i Cabarrocas, P. Engineering island-chain silicon nanowires via a droplet mediated Plateau-Rayleigh transformation. *Nat. Commun.* **2016**, *7*, 12836.
(25) Sun, Y.; Dong, T.; Wang, J.; Xu, J.; Chen, K.; Roca i Cabarrocas, P.; Yu, L. Meandering growth of in-plane silicon nanowire springs. *Appl. Phys. Lett.* **2019**, *114*, 233103.
(26) Xue, Z.; Sun, M.; Dong, T.; Tang, Z.; Zhao, Y.; Wang, J.; Wei, X.; Yu, L.; Chen, Q.; Xu, J.; Shi, Y.; Chen, K.; Roca i Cabarrocas, P. Deterministic line-shape programming of silicon nanowires for extremely stretchable springs and electronics. *Nano Lett.* **2017**, *17*, 7638−7646.
(27) Xu, M.; Wang, J.; Xue, Z.; Wang, J.; Feng, P.; Yu, L.; Xu, J.; Shi, Y.; Chen, K.; Roca i Cabarrocas, P. High performance transparent in-plane silicon nanowire Fin-TFTs via a robust nano-droplet-scanning crystallization dynamics. *Nanoscale* **2017**, *9*, 10350−10357.
(28) Yin, H.; Yang, H.; Xu, S.; Pan, D.; Xu, J.; Chen, K.; Yu, L. High performance Si nanowire TFTs with ultrahigh on/off current ratio and steep subthreshold swing. *IEEE Electron Device Lett.* **2020**, *41*, 46−49.
(29) Hu, R.; Ma, H.; Yin, H.; Xu, J.; Chen, K.; Yu, L. Facile 3D integration of Si nanowires on Bosch-etched sidewalls for stacked channel transistors. *Nanoscale* **2020**, *12*, 2787−2792.
(30) Dong, T.; Sun, Y.; Zhu, Z.; Wu, X.; Wang, J.; Shi, Y.; Xu, J.; Chen, K.; Yu, L. Monolithic integration of silicon nanowire networks as a soft wafer for highly stretchable and transparent electronics. *Nano Lett.* **2019**, *19*, 6235−6243.
(31) Wu, X.; Ma, H.; Yin, H.; Pan, D.; Wang, J.; Yu, L.; Xu, J.; Shi, Y.; Chen, K. 3D Sidewall integration of ultrahigh-density silicon nanowires for stacked channel electronics. *Adv. Electr. Mater.* **2019**, *5*, 1800627.
(32) Tian, B.; Cohen-Karni, T.; Qing, Q.; Duan, X.; Xie, P.; Lieber, C. M. Three-dimensional, flexible nanoscale field-effect transistors as localized bioprobes. *Science* **2010**, *329*, 830−834.
(33) Xu, L.; Jiang, Z.; Qing, Q.; Mai, L.; Zhang, Q.; Lieber, C. M. Design and synthesis of diverse functional kinked nanowire structures for nanoelectronic bioprobes. *Nano Lett.* **2013**, *13*, 746−751.
(34) Kim, S.; Keisham, B.; Berry, V. Cellular nano-transistor: An electronic-interface between nanoscale semiconductors and biological cells. *Mater. Today Nano* **2020**, *9*, 100063.
(35) Sakmann, B.; Neher, E. Patch clamp techniques for studying ionic channels in excitable membranes. *Annu. Rev. Physiol.* **1984**, *46*, 455−472.
(36) Yu, L.; Oudwan, M.; Moustapha, O.; Fortuna, F.; Roca i Cabarrocas, P. Guided growth of in-plane silicon nanowires. *Appl. Phys. Lett.* **2009**, *95*, 113106.
(37) Xue, Z.; Dong, T.; Zhu, Z.; Zhao, Y.; Sun, Y.; Yu, L. Engineering in-plane silicon nanowire springs for highly stretchable electronics. *J. Semicond.* **2018**, *39*, 011001.
(38) He, G.; Hu, N.; Xu, A. M.; Li, X.; Zhao, Y.; Xie, X. Nanoneedle Platforms: The Many Ways to Pierce the Cell Membrane. *Adv. Funct. Mater.* **2020**, *30*, 1909890.
(39) Sun, Y.; Dong, T.; Yu, L.; Xu, J.; Chen, K. Planar Growth, Integration, and Applications of Semiconducting Nanowires. *Adv. Mater.* **2019**, *32*, 1903945.

https://doi.org/10.1021/acs.nanolett.0c04804
Nano Lett. 2021, 21, 2773−2779